J. Fluid Mech. (1981), *vol.* 102, *pp.* 101–126
Printed in Great Britain

A numerical and experimental investigation of the stability of spiral Poiseuille flow

By DONALD I. TAKEUCHI† AND DANIEL F. JANKOWSKI

Department of Mechanical and Energy Systems Engineering, Arizona State University, Tempe, Arizona 85281

(Received 6 June 1979 and in revised form 23 April 1980)

The linear stability of the spiral motion induced between concentric cylinders by an axial pressure gradient and independent cylinder rotation is studied numerically and experimentally for a wide-gap geometry. A three-dimensional disturbance is considered. Linear stability limits in the form of Taylor numbers Ta_L are computed for the rotation ratios $\mu = 0$, 0·2, and $-0{\cdot}5$ and for values of the axial Reynolds number Re up to 100. Depending on the values of μ and Re, the disturbance which corresponds to Ta_L can have a toroidal vortex structure or a spiral form. Aluminium-flake flow visualization is used to determine conditions for the onset of a secondary motion and its structure at finite amplitude. The experimental results agree with the predicted values of Ta_L for $\mu \geqslant 0$, and low Reynolds number. For other cases in which agreement is only fair, apparatus length is shown to be a contributing influence. The comparison between experimental and predicted wave forms shows good agreement in overall trends.

1. Introduction

The hydrodynamic stability problems for circular Couette flow and various parallel shear flows (Poiseuille flows) have received considerable attention in the literature. The various differences between the theoretical and experimental stability characteristics of these flows can be traced to the operative mechanism for instability. For circular Couette flow, the curved streamlines give rise to a centrifugal instability while for parallel shear flows, instability is due to viscosity. If an axial pressure gradient is imposed on the fluid motion between concentric, rotating cylinders, the resulting spiral Poiseuille flow‡, a superposition of Poiseuille flow in an annulus and circular Couette flow, is subject to both mechanisms. By appropriate selection of the flow parameters, the relative importance of the mechanisms can be changed, yielding a spectrum of interesting stability problems. Moreover, the stability characteristics of such a spiral flow have important implications in several applications, e.g. journal bearing lubrication and cooling of rotating machinery.

The externally controllable parameters necessary to characterize spiral Poiseuille flow are conveniently chosen as the radius ratio of the annulus $\eta = a/b$, an axial Reynolds number $Re = \bar{w}(b-a)/\nu$, a Taylor number (rotational Reynolds number) $Ta = \Omega_1(b-a)^2/\nu$, and the ratio of the angular speeds of the cylinders $\mu = \Omega_2/\Omega_1$;

† Present address: AiResearch Manufacturing Company, Phoenix, Arizona.

‡ The terminology is due to Joseph (1976, p. 160) who lists other examples of spiral flow.

0002-1120/81/4609-2760 $02.00 © 1981 Cambridge University Press

here a, b are the radii of the inner and outer cylinders with angular speeds Ω_1, Ω_2, respectively, $\overline{w}$ is the mean axial speed, and ν is the kinematic viscosity of the fluid. With the stability of circular Couette flow as a base, the goal of a linear stability analysis is the smallest value of the Taylor number $Ta_L = Ta_L(\mu, Re, \eta)$ such that, for $Ta > Ta_L$, the basic flow is unstable relative to infinitesimal disturbances. In order to insure that the most unstable disturbance is, in fact, considered, the class of disturbances allowed in the stability problem must not be unduly restricted. For circular Couette flow, it is well-known that the consequence of linear instability is the appearance of a steady finite-amplitude secondary motion consisting of toroidal (axisymmetric) vortices† distributed periodically along the axis of the cylinders. Hence, at least for small Re, it is natural to consider an axisymmetric disturbance. This assumption, together with the restriction to a narrow gap ($\eta \to 1$), were used in the analytical studies by Chandrasekhar (1960, 1962), DiPrima (1960), Krueger & DiPrima (1964), Datta (1965), and Elliot (1973). The restriction to a narrow gap was relaxed by Hasoon & Martin (1977), who considered flows with Reynolds numbers as high as 1000. Hasoon & Martin question the use of a parabolic form for the axial velocity profile in the narrow gap case and advocate the use of an averaged axial velocity profile in the stability problem. A careful discussion of these papers, and specifically the points raised by Hasoon & Martin, is provided by DiPrima & Pridor (1979), whose calculations dispute the conclusions of Hasoon & Martin.

A general conclusion that can be drawn from the available analytical results on the *axisymmetric* problem is that Ta_L increases monotonically with Re, that is, an axial flow stabilizes circular Couette flow. However, it is clear that such a stabilizing effect cannot continue indefinitely, for at large enough Re, the viscous mechanism must lead to instability even without rotation (Mott & Joseph 1968). This idea has been exploited by Hughes & Reid (1968), who, for a narrow gap and an axisymmetric disturbance, generalized the asymptotic methods associated with the Orr–Sommerfeld equation of viscous instability theory.

The first treatment of the stability problem with a general (non-axisymmetric) disturbance is the recent numerical study for an arbitrary gap by Chung & Astill (1977). In this general case, the stability analysis requires two wavenumbers: the (usual) axial wavenumber α introduced by the axial periodicity of the disturbance and an azimuthal wavenumber n, necessarily an integer, introduced by the tangential variation of the disturbance. The linear stability limit is then found by determining the minimum on the family of neutral stability curves generated as α and n vary over the proper ranges. In this regard, the minimization process used by Chung & Astill is difficult to follow and includes the assumption that Ta_L increases monotonically with Re for *all* n. There is no theoretical justification for this assumption so that the treatment of the problem with a general disturbance must be regarded as incomplete. Some additional comments on the minimization process used by Chung & Astill are provided by DiPrima & Pridor (1979).

The most complete experiments on the stability of spiral Poiseuille flow are those of Snyder (1962, 1965) for $\eta = 0{\cdot}95$ and $0{\cdot}96$. They include observations of the wavenumbers near the onset of instability and clearly show that toroidal vortices ($n = 0$) are replaced by spiral vortices ($n \neq 0$) for Re greater than about 15 for $\mu = 0$. Experi-

† This is not necessarily so for $\mu < 0$ (Krueger, Gross & DiPrima 1966).

ments by Schwarz *et al.* (1964) for $\eta = 0{\cdot}95$ and Nagib (1972) and Mavec (1973) for $\eta = 0{\cdot}77$ concentrate on the onset of instability, but also include observations on whether the vortices are toroidal or spiral. The experiments by Gravas & Martin (1978) are concerned solely with the onset of instability.

The experimental observations for circular Couette flow have now been explained by nonlinear theory (e.g. Davey 1962). This analysis establishes that an equilibrium configuration with waveform predicted by the linear theory is the consequence of linear instability. Comparisons of theoretical and experimental results on the stability of spiral Poiseuille flow assume (at least tacitly) a similar equilibrium behaviour although no supporting analysis exists. Once this assumption is made the most satisfying situation occurs when agreement is achieved both on the onset of instability and the corresponding wavenumbers. So long as a toroidal waveform is observed experimentally there is good agreement between Ta_L and the onset of instability for a narrow gap; however, when the wave form assumes a spiral form, the axisymmetric predictions for Ta_L lie above† the corresponding experimental results as do the non-axisymmetric predictions of Chung & Astill (1977) (see figures 3 and 4 in their paper). The pattern is similar for wavenumbers: agreement is reasonable only if a toroidal disturbance is meaningful. The non-axisymmetric wavenumbers of Chung & Astill do not agree with the experimental results of Snyder (1962, 1965). Better comparisons may be possible with a complete treatment of the general stability problem.

The present work is concerned with a numerical and experimental investigation of the linear stability of spiral Poiseuille flow in a wide-gap annulus. The theoretical disturbance is allowed to be three-dimensional, with the proper wavenumbers determined by their correspondence to the minima on numerically generated neutral stability curves. Flow visualization is used to determine the conditions for the onset of a secondary motion and its structure at finite amplitude. The predicted values of Ta_L and the corresponding waveform are compared to the experimental results. Reasons are suggested to explain the nature of the comparison.

2. Problem formulation and solution method

2.1. *Basic flow*

The flow under consideration is the steady, fully-developed flow of an incompressible, Newtonian fluid in the annulus formed by rotating concentric cylinders. If (V_R, V_Θ, V_Z) denote the velocity components in the (R, Θ, Z) directions and P^* denotes the pressure, the basic flow is an elementary solution of the Navier–Stokes system of the form

$$(V_R, V_\Theta, V_Z) = (0, V^*(R), W^*(R)) \tag{1a}$$

and

$$\partial P^*/\partial Z = \text{constant}. \tag{1b}$$

After imposing no-slip conditions at the surfaces of the cylinders, it is readily shown that

$$V^*(R) = AR + B/R, \tag{2a}$$

$$A = \frac{\Omega_2 b^2 - \Omega_1 a^2}{b^2 - a^2}, \quad B = \frac{a^2 b^2 (\Omega_1 - \Omega_2)}{b^2 - a^2}, \tag{2b, c}$$

† Agreement can be improved by using an averaged axial velocity profile in the stability problem (see, e.g., figure 2 in Snyder 1962), but this improvement is clearly artificial.

and

$$W^*(R) = \frac{1}{\rho\nu}\frac{\partial P^*}{\partial Z}\left[R^2 - a^2 + \frac{(b^2-a^2)\ln(R/a)}{\ln(a/b)}\right], \tag{3}$$

where ρ is the fluid density. The solution (2) represents circular Couette flow while the solution (3) is the Poiseuille flow in an annulus.

2.2. *Linear stability analysis*

Following the usual linear stability analysis, the disturbed state is assumed to consist of the superposition of the basic flow and time-dependent infinitesimal disturbance quantities. Thus the disturbed velocity field is

$$(u_r, u_\theta, u_z) = (u', V(r)+v', W(r)+w'), \tag{4}$$

where (u_r, u_θ, u_z) are dimensionless velocity components in the (r, θ, z) directions, $V(r)$ and $W(r)$ are the dimensionless forms of $(2a)$ and (3), and prime denotes a disturbance. The characteristic length and speed used in the non-dimensionalization are $b-a$ and $\bar{w}$, respectively. If the disturbed velocity field and the corresponding pressure field are substituted into the Navier–Stokes system and products of infinitesimal quantities are neglected, the result is a set of linear disturbance equations. An examination of these equations shows that they allow a solution in normal-mode form

$$(u', v', w', p') = [u(r), v(r), w(r), p(r)]\, e^{i[\alpha(z-ct)+n\theta]}, \tag{5}$$

in which t is the dimensionless time, p' is the pressure disturbance, and $u(r)$, $v(r)$, $w(r)$ and $p(r)$ are complex amplitude functions. The axial wavenumber α and the azimuthal wavenumber n characterize the spiral form of the disturbance. For a spatially bounded disturbance, α must be real while azimuthal periodicity requires that n be an integer. With α restricted to positive values the imaginary part of the complex wave speed c determines the stability ($c_i < 0$) or instability ($c_i > 0$) of the basic flow. The condition $c_i = 0$ corresponds to neutral stability. Using the solution form (5), the linear disturbance equations are reduced to

$$\left[i\alpha(W-c)+\frac{inV}{r}\right]u - \frac{2Vv}{r} + \frac{dp}{dr} - \frac{1}{Re}\left(Lu - \frac{2inv}{r^2}\right) = 0, \tag{6a}$$

$$\left[i\alpha(W-c)+\frac{inV}{r}\right]v + \left(\frac{dV}{dr}+\frac{V}{r}\right)u + \frac{inp}{r} - \frac{1}{Re}\left(Lv + \frac{2inu}{r^2}\right) = 0, \tag{6b}$$

$$\left[i\alpha(W-c)+\frac{inV}{r}\right]w + \frac{dW}{dr}u + i\alpha p - \frac{1}{Re}\left(Lw + \frac{w}{r^2}\right) = 0, \tag{6c}$$

and

$$\frac{du}{dr} + \frac{u}{r} + \frac{inv}{r} + i\alpha w = 0, \tag{6d}$$

in which the differential operator L is defined by

$$L \equiv \frac{d^2}{dr^2} + \frac{1}{r}\frac{d}{dr} - \frac{1}{r^2} - \alpha^2 - \frac{n^2}{r^2}.$$

The boundary conditions for the disturbance velocity components follow by imposing no-penetration and no-slip conditions at the cylinder walls. In terms of the complex amplitude functions of (5), these are

$$u = v = w = 0 \quad \text{at} \quad r = \frac{\eta}{1-\eta}, \frac{1}{1-\eta}. \tag{7a,b}$$

The equations (6) and boundary conditions (7) form a linear differential eigenvalue problem which will have a non-trivial solution only for certain values of the parameters. The parameters α, c, n, Re and η appear explicitly while Ta and μ are introduced through the tangential component of the basic velocity. To complete the stability analysis, it is necessary to determine the smallest value of the Taylor number $Ta_L = Ta_L(\mu, Re, \eta)$ such that for $Ta > Ta_L$, the basic flow is unstable, that is, $Ta > Ta_L$ implies $c_i > 0$.

2.3. *Solution method*

The complexity of the eigenvalue problem makes it clear that only a numerical solution is practical. An obvious choice for a numerical procedure is the well-known initial-value method which has an established history in hydrodynamic stability problems (e.g. Sparrow, Munro & Jonsson 1964). Since this method requires values for all of the problem parameters, ultimately a search for particular combinations of these parameters is required to determine Ta_L.

In order to employ standard integration routines, it is convenient to write equations (6) as a system of first-order equations. Moreover, to allow easy treatment of the axisymmetric case ($n = 0$), the pressure variable is eliminated by a transformation due to Roberts (1965). By letting

$$X = Rep - \frac{du}{dr} - \frac{u}{r}, \quad Y = \frac{dv}{dr} + \frac{v}{r}, \quad Z = \frac{dw}{dr}, \tag{8a,b,c}$$

equations (6) can be replaced by

$$\frac{du}{dr} = -\frac{u}{r} - \frac{inv}{r} - i\alpha w, \quad \frac{dv}{dr} = -\frac{v}{r} + Y, \quad \frac{dw}{dr} = Z, \tag{9a,b,c}$$

$$\frac{dX}{dr} = -Re\left[\left[i\alpha(W-c) + \frac{inV}{r}\right]u - \frac{2Vv}{r}\right] - \left(\alpha^2 + \frac{n^2}{r^2}\right)u - \frac{2inv}{r^2}, \tag{9d}$$

$$\frac{dY}{dr} = Re\left[\left[i\alpha(W-c) + \frac{inV}{r}\right]v + \left(\frac{dV}{dr} + \frac{V}{r}\right)u\right] - \frac{2inu}{r^2} + \left(\alpha^2 + 2\frac{n^2}{r^2}\right)v + \frac{n\alpha w}{r} + \frac{inX}{r}, \tag{9e}$$

and

$$\frac{dZ}{dr} = Re\left[\left[i\alpha(W-c) + \frac{inV}{r}\right]w + \frac{dW}{dr}u\right] + \frac{\alpha nv}{r} + \left(2\alpha^2 + \frac{n^2}{r^2}\right)w + i\alpha X - \frac{Z}{r}. \tag{9f}$$

The general solution of the complex system (9) is a linear combination of six linearly independent solution vectors. However, the general solution is not required since, by a judicious choice of initial conditions, it is possible to numerically generate three linearly independent solutions which obey the boundary conditions (7*a*). If a linear combination of these vectors is required to satisfy the remaining conditions (7*b*), the

requirement for a non-trivial solution is the vanishing of a 3×3 determinant (DiPrima & Pridor 1979); symbolically

$$D(Ta, Re, \mu, \eta, c, \alpha, n) = 0. \tag{10}$$

Since this determinant is complex-valued, two parameters must be selected as eigenvalues. Convenient choices are the Taylor number Ta and wave speed c_r. Since a single geometry is considered and c_i is fixed at the neutral stability condition ($c_i = 0$), the values of Ta and c_r which satisfy the condition (10) will vary with μ, Re, α and n; these values will be denoted by Ta^* and c_r^*. The linear stability limit Ta_L is the minimum value of Ta^* as α and n vary over the proper ranges, that is, it is the minimum on a family of neutral stability curves. Mathematically, this condition is the product of successive minimization processes

$$\overline{Ta}(n; \mu, Re) = \min_{\alpha > 0} Ta^*(\alpha; n, \mu, Re), \tag{11}$$

$$Ta_L(\mu, Re) = \min_{n = \text{integer}} \overline{Ta}(n; \mu, Re). \tag{12}$$

For each of the eigenvalue pairs $(\overline{Ta}, \overline{c_r})$ and (Ta_L, c_{rL}), the corresponding values for α and n are identified in an obvious way.

The first step in the solution procedure is the determination of the elements of the characteristic determinant (10). This step is accomplished by a fourth-order, variable step-size, Runge–Kutta integration with an imposed minimum of 100 steps over the unit integration interval. The computations were performed in double precision on a UNIVAC 1100/42 computer. Each evaluation of (10) requires three integrations of 12 real first-order differential equations. At $r = 1/(1-\eta)$, the complex elements required in (10) are reformulated and the determinant is evaluated. The next step involves the simultaneous adjustment of Ta and c_r so as to drive the determinant to zero.

In order to initiate the computations, estimates for the eigenvalues are needed. Since, at the start of this work, no applicable results for the stability of spiral Poiseuille flow relative to a general disturbance were available, some preliminary numerical work was required to obtain reliable initial estimates. They were obtained by advancing, in small increments of the parameters, from limiting cases available in the literature (Krueger & DiPrima 1964; Krueger *et al.* 1966). For an initial search with new extrapolated estimates for the eigenvalues the Box search method (Kuester & Mize 1973, p. 368) was used. This routine was found to iterate very consistently to the vicinity of (Ta^*, c_r^*). Once approximate values were determined, either the Muller method (Muller 1956) or a modified version of the method of steepest descent (Lance 1959) was used to achieve final convergence. Each of these methods had drawbacks. The Muller method was, in some cases, extremely sensitive to the initial estimate; this behaviour could not be predicted *a priori*. The modified method of steepest descent had a much slower rate of convergence. Successful determination of the eigenvalues was the result of considerable numerical experimentation.

Completion of the process just described yields a *single* point on a neutral stability curve. The establishment of a complete curve requires that the process be repeated for various values of α. In certain cases treated in this work, these curves were found to have inflection points but no evidence of the existence of more than a single minimum,

such as reported by DiPrima & Pridor (1979), was observed. In the neighbourhood of $\overline{Ta}$, eigenvalues Ta^* were determined for increments in α of 0·01. The smallest calculated value of Ta^* was taken to be $\overline{Ta}$. The process is next repeated for various integer values for n, providing a sequence of values for $\overline{Ta}$. The minimum of this sequence is Ta_L. While the method for determining Ta_L could be completely automated, it is too subtle for convenient programming and the cost in computer time would be excessive. Therefore only (Ta^*, c_r^*) were determined entirely on the computer.

The numerical procedures and computer code were verified by comparison with selected results from the literature (Krueger & DiPrima 1964; Krueger *et al.* 1966; DiPrima & Pridor 1979). The agreement is quite good in all cases; the detailed comparisons are available in Takeuchi (1979). A second verification is provided by a theoretical result due to Joseph & Munson (1970). They have shown, in the present notation, that

$$Ta_L(\alpha_L, n_L) = Ta_L(-\alpha_L, -n_L). \tag{13}$$

Independent calculations of both sides of (13) showed agreement to the accuracy of the computer.

3. Numerical results

As a practical matter, it is necessary to limit the ranges of the flow parameters for which the calculations are carried out. Since parallel numerical and experimental studies were performed, these ranges were influenced by the anticipated character of the instability. The experimental apparatus was designed on the premise that the instability phenomena of spiral Poiseuille flow would be similar to that of circular Couette flow up to $Re = 200$. The calculations were restricted to a narrower range, $0 \leqslant Re \leqslant 100$. In addition to the usually treated case of a stationary outer cylinder ($\mu = 0$), the values of $\mu = -0{\cdot}5$ and $0{\cdot}2$ were chosen as representative values for counter rotation and co-rotation, respectively. The radius ratio $\eta = 0{\cdot}5$ was chosen since, at the start of this investigation, results for a wide-gap geometry were not available in the literature.

With the physical parameters of the problem chosen, it is only necessary to establish the appropriate ranges for the wavenumbers α and n. The result (13) shows that it suffices to consider $\alpha > 0$ so long as n is allowed to be both a positive and negative integer. There does not appear to be any theoretical way to exclude either negative or positive n for a *general* spiral flow. For spiral Poiseuille flow, Chung & Astill (1977) argue in favour of positive n by using experimental evidence (Snyder 1965) that the inclination of the disturbance spiral is opposite to that of the basic flow at the outer cylinder. In contrast, for the spiral flow formed by superimposing a rigid-body rotation on Hagen–Poiseuille flow, it has been shown that negative n is pertinent (Maslowe 1974; Mackrodt 1976). The same conclusion is drawn for a complicated spiral wake flow by Lessen, Singh & Paillet (1974). Since the arguments are persuasive in each case, the proper choice for n must be associated with some element of the basic flows. With this interpretation, the spiral flows treated by Mackrodt and Lessen *et al.* must have a common feature which is somehow different from that for spiral Poiseuille flow. While a precise determination of this feature has not been attempted, the ideas of Joseph (1976, cha. 6) suggest a connection with the well-known Rayleigh criterion.

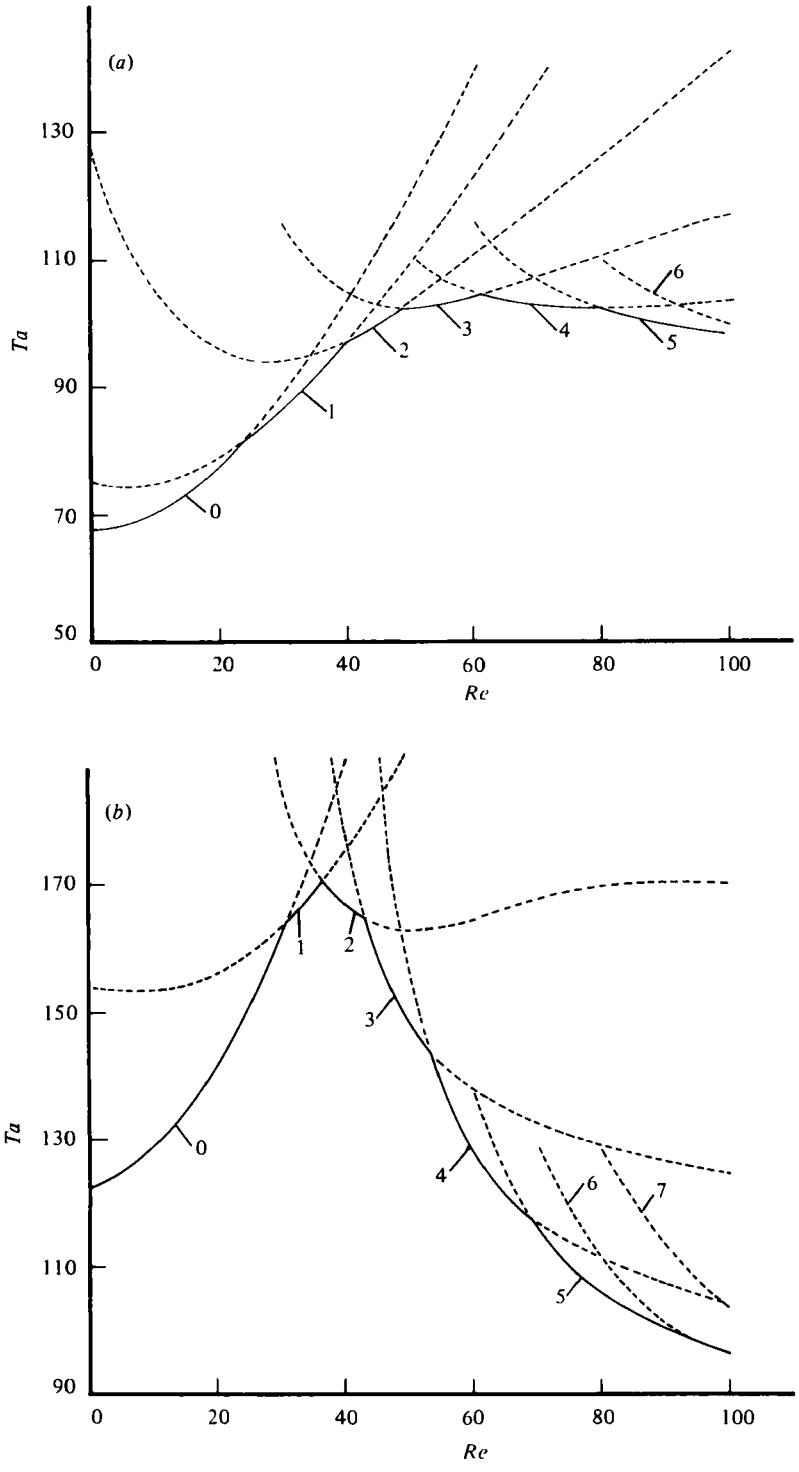

FIGURE 1 (*a*, *b*). For legend see facing page.

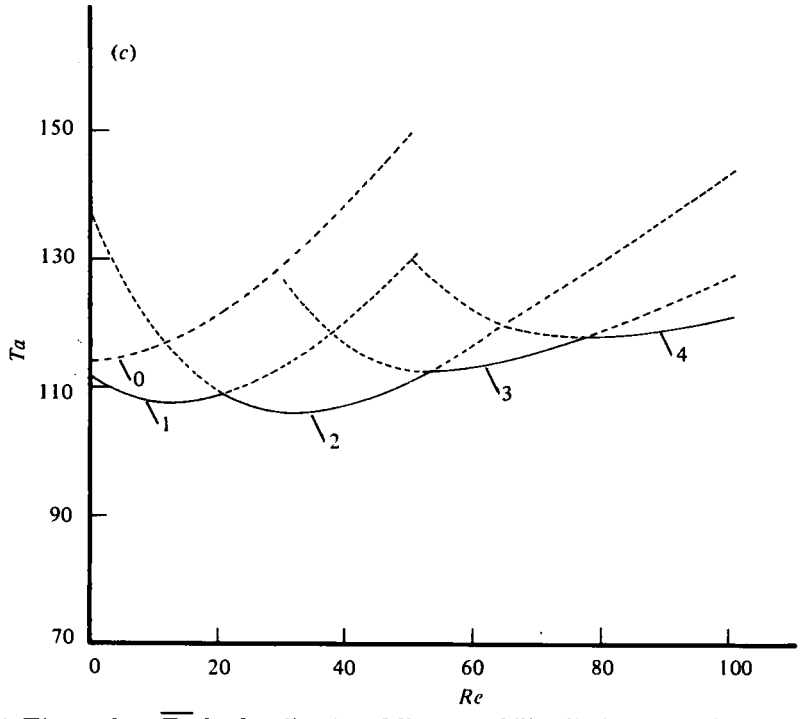

FIGURE 1. Eigenvalues $\overline{Ta}$ (broken lines) and linear stability limit Ta_L (solid line) as a function of Re. The integers identify values of the azimuthal wavenumber; (*a*) $\mu = 0$; (*b*) $\mu = 0{\cdot}2$; (*c*) $\mu = -0{\cdot}5$.

	$\mu = 0$				$\mu = 0{\cdot}2$				$\mu = -0{\cdot}5$			
Re	Ta_L	α_L	n_L	c_{rL}	Ta_L	α_L	n_L	c_{rL}	Ta_L	α_L	n_L	c_{rL}
1	68·21	3·17	0	1·181	124·8	3·15	0	1·181	110·8	4·07	1	9·498
10	70·67	3·17	0	1·180	129·3	3·15	0	1·180	107·8	3·88	1	1·945
20	77·84	3·19	0	1·176	142·5	3·17	0	1·177	108·7	3·63	1	1·548
30	86·82	3·50	1	1·469	163·0	3·20	0	1·172	106·2	4·31	2	1·543
40	97·01	3·54	1	1·418	166·6	4·20	2	2·215	107·4	4·05	2	1·457
50	102·6	4·31	3	1·787	148·5	4·11	3	2·353	111·4	3·79	2	1·414
60	104·1	3·95	3	1·736	128·7	3·92	4	2·388	113·5	4·51	3	1·445
70	102·7	3·95	4	1·834	116·1	3·84	5	2·392	116·0	4·17	3	1·423
80	102·0	4·02	5	1·900	106·1	3·32	5	2·296	118·2	4·70	4	1·452
90	99·56	3·60	5	1·875	100·3	2·93	5	2·241	119·2	4·34	4	1·440
100	98·16	3·24	5	1·865	96·57	2·62	5	2·208	121·1	4·02	4	1·434

TABLE 1. Linear stability limit Ta_L and corresponding α_L, n_L, and c_{rL} as a function of μ and Re.

According to this criterion, the flows considered by Mackrodt and Lessen *et al.* have *stable* tangential velocity components while in the work of Chung & Astill, they are *unstable*. Thus a tentative conclusion is that the sense of the disturbance spiral (i.e. the sign of n) depends on the stability characteristics of the tangential component of the spiral flow. Since, in the present work, the chosen values of μ all yield an *unstable* tangential component, this implies that n should be restricted to *positive* values. As a

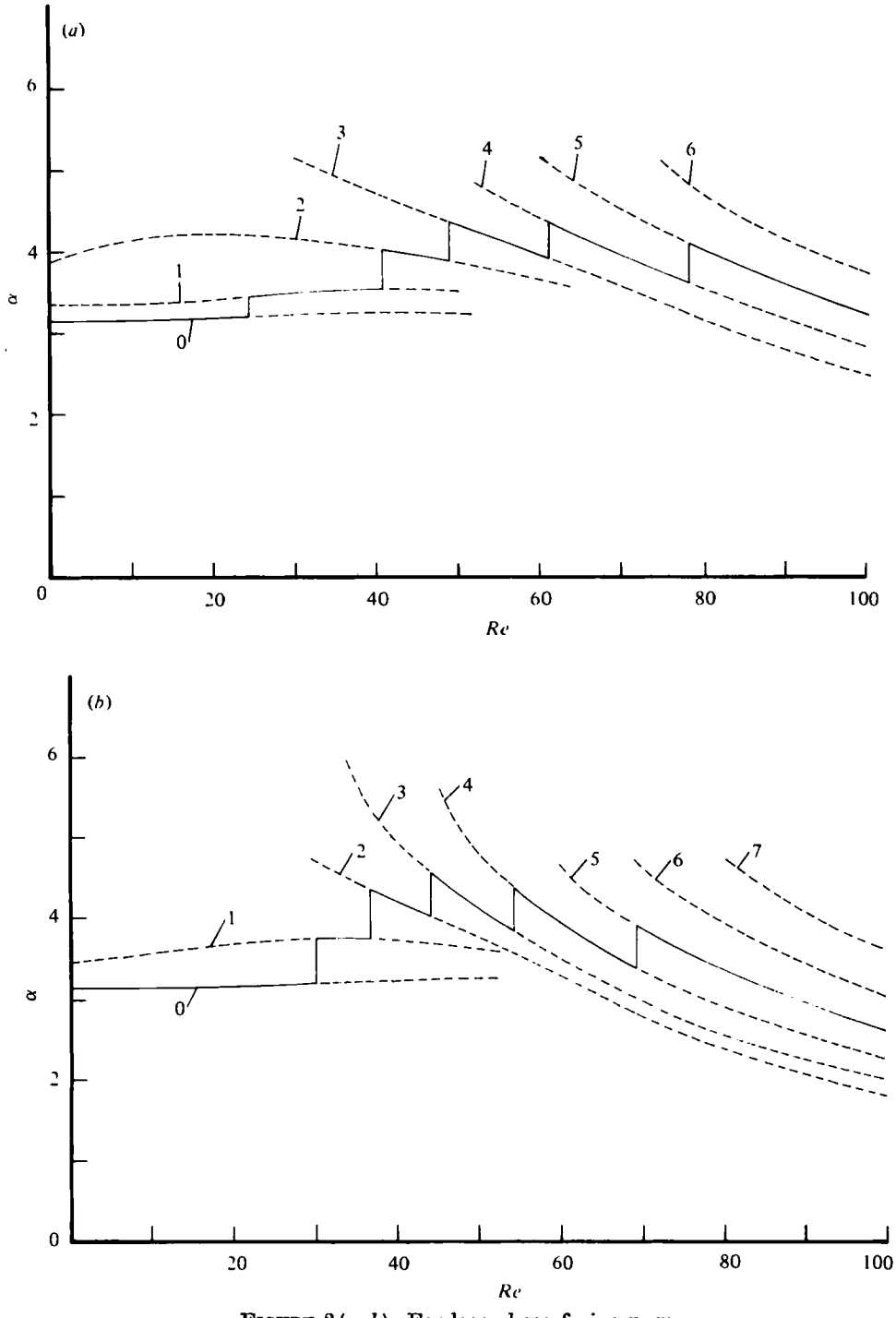

FIGURE 2 (*a*, *b*). For legend see facing page.

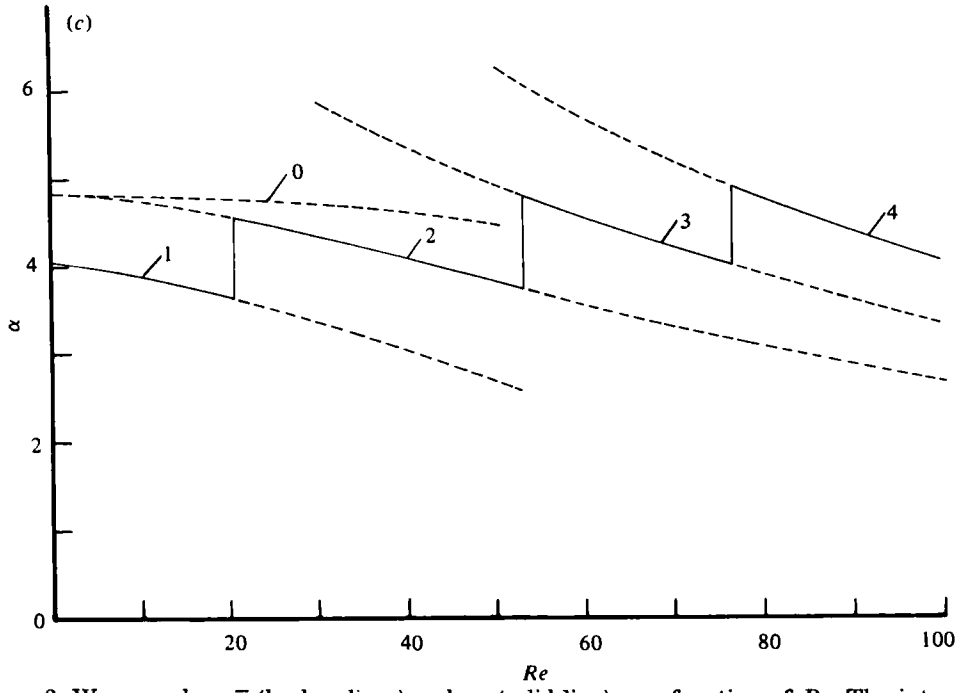

FIGURE 2. Wavenumbers $\bar{\alpha}$ (broken lines) and α_L (solid line) as a function of Re. The integers identify values of the azimuthal wavenumber; (*a*) $\mu = 0$; (*b*) $\mu = 0{\cdot}2$; (*c*) $\mu = -0{\cdot}5$.

test of this choice, the eigenvalues $\overline{Ta}(-n;\mu,Re)$ were compared with the eigenvalues $\overline{Ta}(n;\mu,Re)$ for $n = 1, 2$, $\mu = 0$ and $Re = 1, 50, 100$. The smallest eigenvalue corresponded to $n > 0$ in each case.

With the parameters established, a large number of neutral stability curves were generated by the numerical procedures discussed in §2. With the help of these curves, the eigenvalues $\overline{Ta}(n;\mu,Re)$ were obtained. For the sake of completeness, all of the computed values of $\overline{Ta}(n;\mu,Re)$† are shown in figure 1. These figures clarify the dependence of Ta_L on n and clearly show that Ta_L does not increase monotonically with Re for a general disturbance. In each of the figures, the solid portions of the smooth curves give Ta_L as a function of Re. A significant feature is the continuous, but not smooth, nature of these solid curves. The dashed portions of the smooth curves represent solutions to the linear stability problem which are necessary solely to insure the proper selection of Ta_L. Table 1 lists Ta_L and the corresponding values of c_{rL}, α_L and n_L. Complete results of this form, which clearly illustrate the importance of a systematic treatment of all pertinent values of n, have not been reported previously.

The results for $\mu = 0$ and $0{\cdot}2$ (figures 1*a*, *b*) show that, for small Reynolds number, the disturbance is toroidal ($n = 0$). On the other hand for $\mu = -0{\cdot}5$ (figure 1*c*) the disturbance has a spiral form for all Re considered. Another common feature of the $\mu = 0$ and $0{\cdot}2$ cases is the stabilizing effect as Re increases from zero. In both cases this is followed by a decrease in stability, with the decrease for $\mu = 0{\cdot}2$ quite pronounced. In contrast, the counter-rotation case of figure 1(*c*) shows a destabilization as Re increases from zero while for higher Re the trend is toward increased stability.

† Tables of these values are available in Takeuchi (1979) or on request to the authors.

	Present work			Chung & Astill (1977)		Hasoon & Martin
Re	$n = 0$	$n = 1$	$n = 2$	$n = 0$	$n = 1$	$n = 0$
		$\overline{Ta}$		$\overline{Ta}$		$\overline{Ta}$
10	70·67†	75·22	105·6	70·67		70
20	77·84†	79·30	96·32	77·90		75
50	120·5	109·2	103·2	120·8	114·2	113
		$\bar{\alpha}$		$\bar{\alpha}$		
10	3·17†	3·37	4·14	3·19		
20	3·19†	3·43	4·21	3·074		
50	3·26	3·52	3·89	2·96	2·51	
		$\bar{c}_r$		$\bar{c}_r$		
10	1·180†	1·928	3·033	1·180		
20	1·176†	1·578	2·053	1·174		
50	1·158	1·391	1·598	1·15	1·48	

† Corresponds to Ta_L.

TABLE 2. Comparison of present results with available results for $\mu = 0$ and $\eta = 0{\cdot}5$.

The results shown in figure 1 also serve to identify n_L as a function of *Re*. With n_L known, the proper values of α_L and c_{rL} can be selected from the calculated values of $\bar{\alpha}$ and $\bar{c}_r$. The results for α_L are shown in figure 2. The dashed and solid portions of the curves in these figures correspond to the dashed and solid portions of the curves in figure 1. Note that double values of α_L and c_{rL} (i.e. non-simple eigenvalues) correspond to the discrete changes in n_L.

The variations of α_L and c_{rL} with *Re* for $\mu = 0$ and 0·2 exhibit similar general trends which are different from those for $\mu = -0{\cdot}5$. This pattern of similarity between results for $\mu = 0$ and 0·2 and contrasting results for $\mu = -0{\cdot}5$ was observed earlier in the dependence of Ta_L on *Re*.

The only available stability calculations for spiral Poiseuille flow in a geometry with $\eta = 0{\cdot}5$, which overlap the parameters of the present study, are those of Hasoon & Martin (1977) and Chung & Astill (1977). These authors restrict the range for the azimuthal wavenumber and thus their eigenvalues do not, in all cases, correspond to the linear stability limit Ta_L. However, a comparison can be made with the 'intermediate' eigenvalues $\overline{Ta}$. In terms of the present notation, this comparison is presented in table 2. The axisymmetric results of Hasoon & Martin are based on the use of an averaged axial velocity distribution and are obtained by a Galerkin method. Note that the present calculations for $\overline{Ta}$ yield higher values, with the difference increasing with *Re*. A similar difference is noted by DiPrima & Pridor (1979) for $\eta = 0{\cdot}95$; they attribute it to the fact that the use of an averaged axial velocity profile is inappropriate. Hasoon & Martin do not give any results for α and c_r that are pertinent to the present discussion.

The numerical solution method of Chung & Astill (1977) is essentially equivalent to that of the present work *up to the point of extracting the eigenvalues from an eigenvalue determinant*. The fact that a slightly different treatment of the initial-value problem

leads them to a 6×6 determinant rather than a 3×3 determinant is unimportant. The earlier comments show that the process of determining Ta_L requires careful implementation. The eigenvalue extraction process used by Chung & Astill is difficult to follow and appears to have been designed to obtain Ta_L directly without the extensive intermediate calculations used here. Hence it was not possible to identify specific reasons for the limited agreement for $n = 0$ (note $\bar{\alpha}$) and the lack of agreement for $n = 1$ shown in table 2. A possibility is suggested by DiPrima & Pridor (1979) who compare their calculations for $\eta = 0{\cdot}95$ and $n = 0$ with those of Chung & Astill. They note a similar limited agreement and suggest that, in some cases, the eigenvalues reported by Chung & Astill might not correspond to the minimum on a neutral stability curve. This thought is reinforced by the listing of 'probable eigenvalues' by Chung & Astill. Experience gained during the present work indicates that the minimization process becomes more delicate as n increases. This may be a contributing factor to the discrepancies for $n = 1$.

An important comment can be made that bears on the *overall* validity of the calculations performed by Chung & Astill. They assume that Ta_L increases monotonically with Re for *all* n and indeed it seems that this assumption is built into their eigenvalue iteration procedure. While there is ample theoretical evidence to support this assumption for $n = 0$, the present results (figure 1) all show that, for $\eta = 0{\cdot}5$, the assumption is incorrect. Thus it seems clear that Chung & Astill failed, in some cases, to consider sufficiently high azimuthal wavenumbers.

4. Experimental apparatus and procedures

4.1. *Experimental apparatus*

The basis for the design of the experimental apparatus was the expected nature of the instability. It is known, from nonlinear theory (e.g. Davey 1962) that the result of linear instability for circular Couette flow is the establishment of an equilibrium configuration with finite amplitude that depends on $Ta - Ta_L$. This important characteristic explains the success of relatively simple visualization experiments (Coles 1965) in verifying the linear stability predictions for circular Couette flow. For some *unknown* range of Re, it is reasonable to suppose that this characteristic is also present for spiral Poiseuille flow in a wide-gap geometry. For the present work the assumption was made that this range would extend at least up to $Re = 200$. For such moderate Re, it was anticipated that a successful experimental program could be based on aluminium-flake flow visualization. This technique affords a simple and economical means for the determination of the onset of instability. It also provides a way to examine the structure of the anticipated equilibrium configuration.

An experimental apparatus with provision for inducing an axial flow in the annulus formed by concentric rotating cylinders was designed and constructed. A schematic diagram of the apparatus is shown in figure 3.

The annular flow passage is formed by independently mounted and driven cylinders. Commercially available glass cylinders with nominal 4 inch inside diameters were used to fabricate the outer cylinder. Thus, for $\eta = 0{\cdot}5$, the inner cylinder is required to have a diameter of 2 inches. To insure fully-developed axial and tangential velocity profiles, the length of the flow passage was made as large as could be accommodated in the

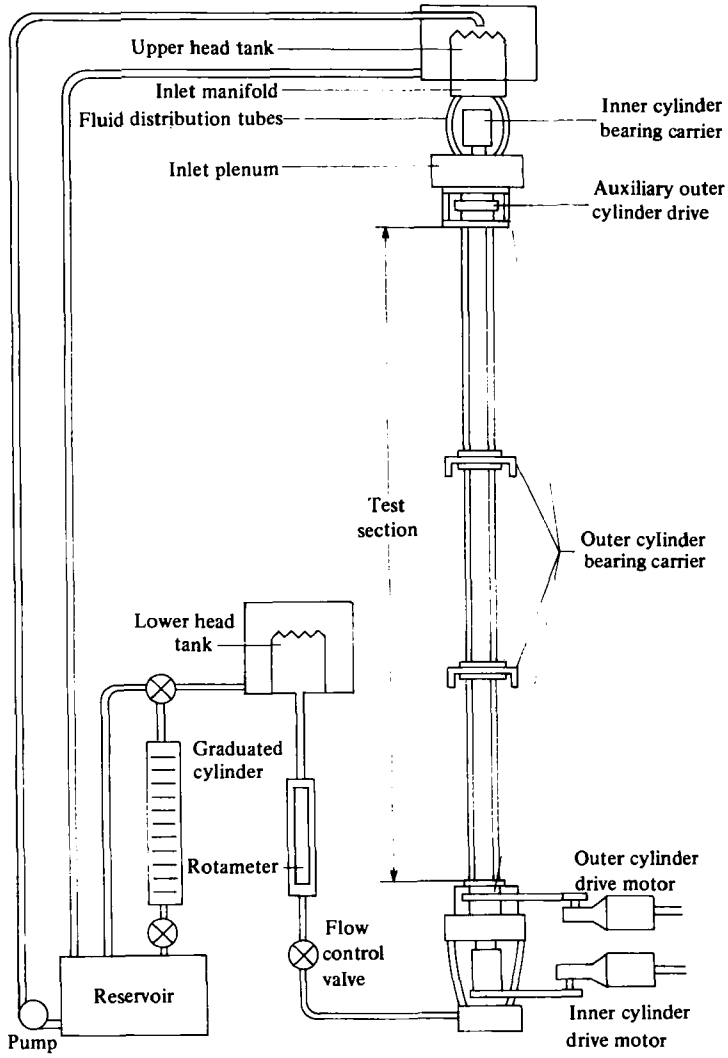

FIGURE 3. Schematic diagram of experimental apparatus.

available laboratory space. This length exceeds the maximum estimated entrance length (Sparrow & Lin 1964; Martin & Payne 1972) by a considerable margin.

The outer cylinder is fabricated from several components which provide drive sections at either end and a transparent test section. The transparent portion of the outer cylinder consists of three $4{\cdot}003 \pm 0{\cdot}003$ inch precision bore, borosilicate glass cylinders obtained from Fischer Porter and Company. Polycarbonate flanges were bonded to the ends of each cylinder and machined concentric to the inside bore. The two interior flange junctions are supported by ball bearings. The bearing support platforms are, in turn, attached to a vertical structural member. The combined length of the glass cylinders, and hence the useful length of the flow passage for visualization purposes, is 102·50 inches. Including the drive sections, the total length

of the outer cylinder is 115·25 inches. In contrast, a simpler design was possible for the inner cylinder. It is a single-piece pump shaft 2·0000 ± 0·0005 inches in diameter. The experimental radius ratio is thus 0·4996 ± 0·0004.

To aid in alignment of the inner and outer cylinders, all bearing mounts possess adjusting mechanisms for 6 degrees of freedom. In addition, the upper-cylinder bearing supports are traverse mounted to allow runout determination following the completion of alignment procedures. The outer cylinder can be separated at any of its flanged connexions and the upper portion raised to provide access to the inner cylinder without affecting alignment. Both cylinders have slip connections to allow inner cylinder access and to compensate for thermal expansion. The final measured runout of the inner cylinder is 0·012 inches maximum at approximately its centre. The maximum runout of the bore of the outer cylinder is 0·0015 inches. Including dimensional tolerances, this gives a combined maximum gap variation of 1·7 %.

All cylinder drive components utilize timing belts and sprockets to eliminate rotation-rate variation due to slippage. The cylinder rotation-rates can be independently controlled with separate, variable-speed drive motors and controllers. For the results to be reported here, the cylinders were directly coupled for $\mu = -0{\cdot}5$ and 0·2 and driven by a single motor and controller. Speed regulation is held to ± 0·5 % by incorporating a feedback control system. An electronic timer, controlled by microswitches, provides a means of determining cylinder rotation-rates.

The axial fluid flow is maintained by a gravity-feed, constant-head system as sketched in figure 3. Fluid is pumped from a reservoir into the upper head tank by a progressive cavity pump driven by a variable speed motor. A constant pressure head is maintained by a continuous flow over a weir assembly in the upper head tank. A manifold attaches directly to the upper head tank and distributes the fluid to the inlet plenum through four flexible tubes. The inlet plenum incorporates a screen and flow straightener to aid the establishment of a circumferentially uniform flow. The fluid enters the annular flow passage through a smooth entry bell, flows down the annulus, and into an exit plenum. It then flows through four flexible tubes into a collector. Provisions for temperature measurements are incorporated into the entrance manifold and exit collector. The fluid flows from the collector through a flow-regulating valve, a flow meter and into the bottom of the lower head tank. The flow meter serves only as a visual indicator to aid in valve adjustments. Overflow from the lower head tank is returned to the reservoir through the flow measurement system. A precision bore graduated cylinder collects the fluid for a timed volumetric measurement.

A silicone oil (Dow Corning 200 fluid) was selected as the working fluid because of its chemical inertness and stable kinematic viscosity. A nominal value for ν of 10 centistokes was found to be suitable for the ranges of parameters considered. The actual value of ν depends on the fluid temperature. This dependence was obtained with a Saybold Universal Viscometer to an accuracy of 0·5 % over the range of operating temperatures. Temperatures were determined by ASTM thermometers with a smallest scale division of 0·05 F°. For the purpose of flow visualization, aluminium powder was added to the silicone oil after straining through a screen with a mesh opening of 0·0029 inches. The addition of the aluminium powder caused no detectable change in ν.

4.2. *Experimental procedures*

The first phase of the experimental effort focused on the determination of the critical Taylor number Ta_c corresponding to the observed onset of instability. For given μ, its value depends on Re. Thus it is necessary to measure three quantities: the angular speed of the inner cylinder at the onset of instability Ω_{1c}, the volume flow rate Q, and the fluid temperature. With these quantities known,

$$Ta_c = \frac{\Omega_{1c}(b-a)^2}{\nu} \tag{14}$$

and

$$Re = \frac{Q}{\pi(b+a)\nu}. \tag{15}$$

It is expected that, up to some unknown value of Re, Ta_c will equal Ta_L. The second phase consisted of measurements of the axial wavelength and angle of inclination of the expected equilibrium wave form. These measurements lead to the critical wavenumbers α_c and n_c.

Critical Taylor number. The *definition* of a criterion for the onset of instability followed some preliminary observations. For the special case $Re = 0$, the initial signs of instability are observed in the central portion of the test section. A small increase in Ω_1 then results in a vortex structure along the entire length of the test section. Due to the presence of suspended aluminium flakes, this structure is characterized by alternate light and dark bands (Coles 1965). For low Reynolds numbers, the vortex development is similar. For higher Re, however, the upstream propagation of disturbances is apparently inhibited and a vortex structure along the entire length of the test section was not observed. In these cases, a stable vortex structure fills the lower portion of the test section while a region at the start of the test section remains void of visible disturbances. With further increases in Ω_1, it was possible to increase the length of the vortex structure. A sequence of the observed states is shown schematically in figure 4.

Based on the preliminary observations and the supposition that developing spiral Poiseuille flow is more stable than the fully-developed basic flow (Martin & Hasoon 1976), the critical condition is defined as *the occurrence of a persistent vortex structure which fills the test section downstream of the general region in which a disturbance is first observed.* In general, as Re increases, the length of this vortex structure decreases until, at sufficiently high Re, vortices are first observed near the exit of the test section.

Following the definition of the stability criterion, the experiments were carried out for the previously chosen values of μ and $0 \leqslant Re \leqslant 150$. With the value of μ fixed, Re is set to the desired value by adjusting the flow control valve. Then Ω_1 is set at a value somewhat lower than the anticipated critical value and increased in small steps. It was found that the specified 0·5 % accuracy of speed control is not attained without a warm-up period of approximately 1 h. Due to the normal vertical temperature gradient in the laboratory, considerable temperature drift is observed following a cold start. Approximately 2 h are required for the apparatus to attain temperature equilibrium. Once speed regulation and thermal equilibrium have been established, the test sequence proceeds with flow rate and temperature measurements at each value of Ω_1. The average temperature between the entrance manifold and exit collector was used to determine ν. At thermal equilibrium, the temperature at these locations

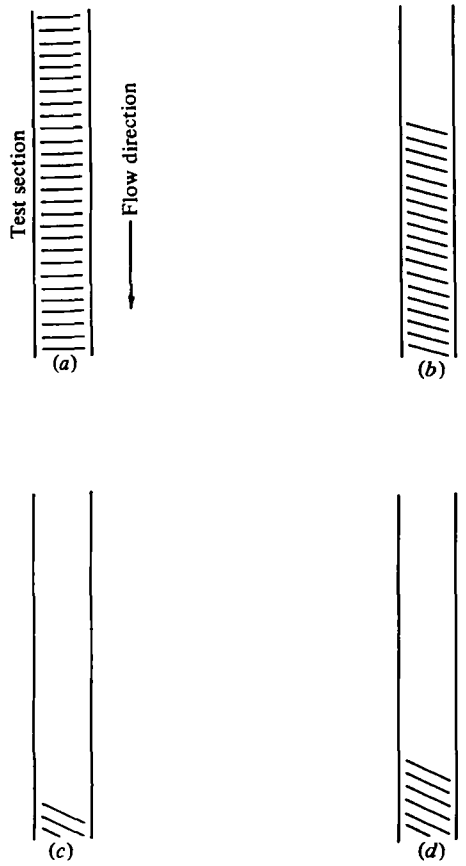

FIGURE 4. Sequence of observed states: (*a*) low *Re*, $\Omega_1 = \Omega_{1c}$; (*b*) intermediate *Re*, $\Omega_1 = \Omega_{1c}$; (c) high *Re*, $\Omega_1 = \Omega_{1c}$; (*d*) same *Re* as (c), $\Omega_1 > \Omega_{1c}$.

differed by at most 0·1 F°, except for the lowest *Re*. Incremental increases in Ω_1 were generally held to less than 1 % of the expected critical value. The measured values of Ω_1 are estimated to have an uncertainty of 0·5 %; the uncertainty in Q is estimated to be 1·7 %. The total uncertainties in Ta_c and *Re* are then computed as 1·0 % and 1·8 %, respectively. The reproducibility of Ω_{1c} was tested by repeating selected data points and by using an alternate procedure with Ω_{1c} approached from above. In all cases, Ω_{1c} was found to be reproducible within the experimental uncertainty.

The stability criterion is adequate only if natural convection effects are not present. It was found that these effects are troublesome only at very low *Re* or if thermal equilibrium of the apparatus has not been achieved. For the great majority of the data taken, the basic axial velocity dominates any convection-induced velocity so that the influence of natural convection is insignificant. The occurrence of such effects was easily recognized since the resulting disturbances had a constantly changing wave form and would appear at values of Ω_1 much lower than the expected critical value.

Critical wave form. The critical vortex structure can be toroidal or spiral, depending on the value of *Re*. Experimentally this structure can be characterized by an axial wavelength s and an angle of inclination relative to the horizontal ψ_c. These quantities

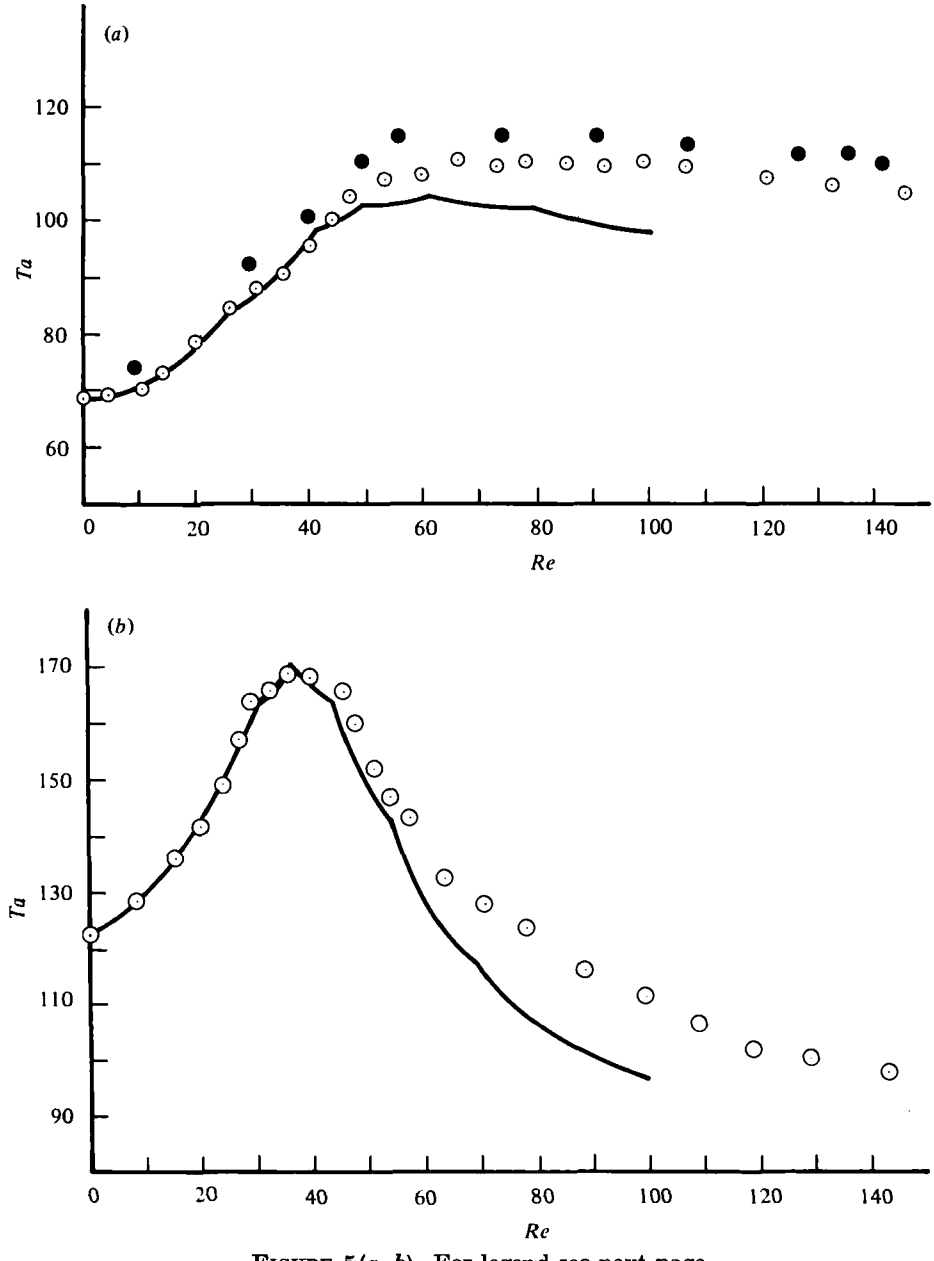

FIGURE 5(a, b). For legend see next page.

lead to α_c and n_c. Ideally, up to some unknown value of Re, $\alpha_c = \alpha_L$ and $n_c = n_L$. The original idea was to base ψ_c and s measurements on photographs of the critical wave form. However, it was very difficult to obtain adequate photographs. At low and intermediate Reynolds number, an increase in Ω_1 above Ω_{1c} was required to increase the intensity, and hence the resolution, of the vortex wave form. A similar increase was necessary at high Reynolds number, where vortices are first observed at the exit of the test section, to ensure both adequate resolution and visible length of the wave form.

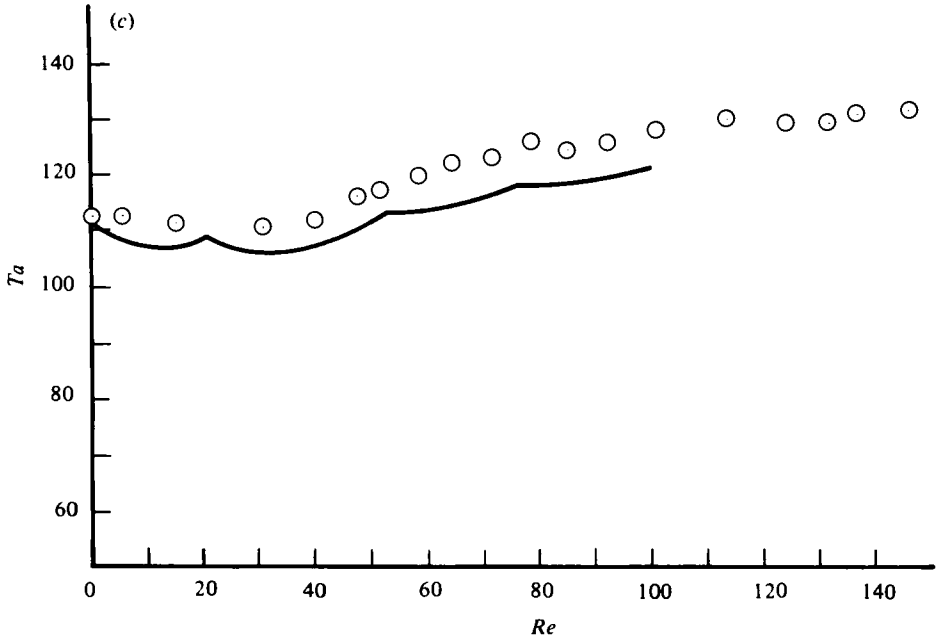

FIGURE 5. Comparison of Ta_c and Ta_L (solid line); (*a*) $\mu = 0$ (●, 'shortened' apparatus; see §6); (*b*) $\mu = 0{\cdot}2$; (*c*) $\mu = 0{\cdot}5$.

Since ψ_c and s could not be conveniently determined at Ω_{1c}, photographs were taken at $\Omega_1 = 1{\cdot}05\,\Omega_{1c}$. A similar approach was used by Snyder (1962). For a given μ, Ta_c was determined for the entire range of Re; this was followed by the independent determination of ψ_c and s over a smaller range, $0 \leqslant Re \leqslant 100$.

Axial wavelengths were measured from the photographs. To eliminate errors due to camera-lens distortion, measurements were referenced to a scale included in each photograph. The estimated uncertainty for the corresponding axial wavenumber $\alpha_c = 2\pi/s$ is 3·0%. In some cases, the angles of inclination are not discernible in the photographs, even for $\Omega_1 = 1{\cdot}05\,\Omega_{1c}$. Rather than increase Ω_1 further, angles were measured directly with an adjustable protractor. The corresponding azimuthal wavenumber is

$$n_c = \frac{2b}{s}\tan\psi_c. \tag{16}$$

The estimated uncertainty in n_c is ± 1.

Some preliminary observations of the wave forms at $\Omega_1 = 1{\cdot}05\,\Omega_{1c}$ showed that they are not, in all cases, reproducible within the experimental uncertainty. Hence the lack of repeatibility of ψ_c and s can be attributed to a small measurement error and a possibly large variation due to non-reproducibility of the wave form.

5. Experimental results and comparisons

The experiments to determine Ta_c were carried out to $Re = 150$. This range was sufficient to test the predictions and establish the values of Re for which $Ta_c = Ta_L$. Experimental results are shown in figure 5 along with the corresponding predictions

$\mu = 0$		$\mu = 0{\cdot}2$		$\mu = -0{\cdot}5$	
Re	Ta_c	Re	Ta_c	Re	Ta_c
0	68·6	0	112·6	0	112·4
4·2	69·4	8·3	128·7	5·7	112·7
10·2	70·4	15·2	136·3	15·2	111·4
14·0	73·4	19·9	141·9	30·9	110·6
19·7	77·7	23·6	149·1	40·0	111·9
25·9	84·7	26·8	157·1	47·6	116·2
30·6	88·2	29·3	163·8	51·7	117·2
35·3	90·1	32·3	165·7	58·5	119·8
40·0	95·7	35·5	168·9	64·6	122·0
43·9	100·4	39·6	168·3	71·5	123·0
46·8	104·5	45·3	166·0	78·4	125·8
53·1	107·5	47·6	160·1	84·8	124·3
59·5	108·2	50·8	152·0	91·9	125·4
66·2	110·8	54·1	147·1	100·8	127·7
73·2	109·6	57·2	143·5	113·1	129·8
78·0	110·5	63·3	132·9	124·0	129·2
85·4	111·3	70·4	128·3	131·5	129·2
92·4	109·6	78·0	124·1	136·4	130·7
98·7	110·5	88·4	116·2	145·8	131·3
106·2	109·6	99·1	111·7		
120·5	107·8	108·8	106·6		
132·5	106·5	118·3	102·1		
145·4	105·2	128·9	100·6		
		142·7	97·7		

TABLE 3. Critical Taylor number Ta_c as a function of μ and Re.

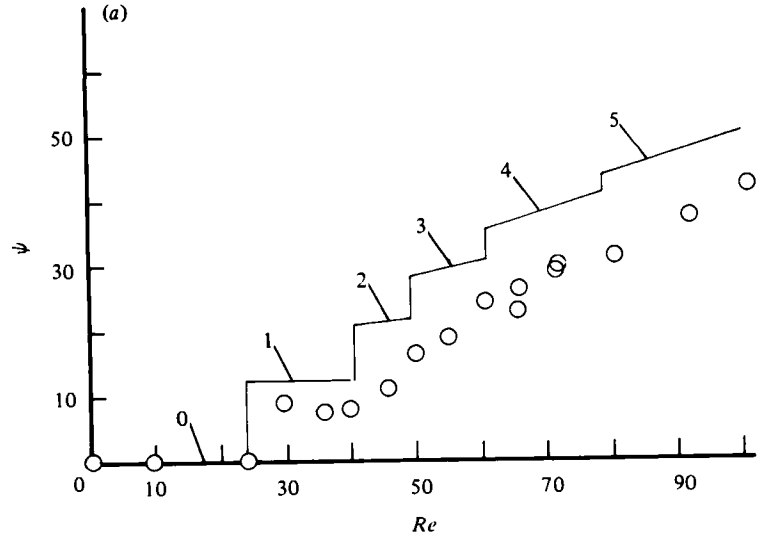

FIGURE 6(a). For legend see next page.

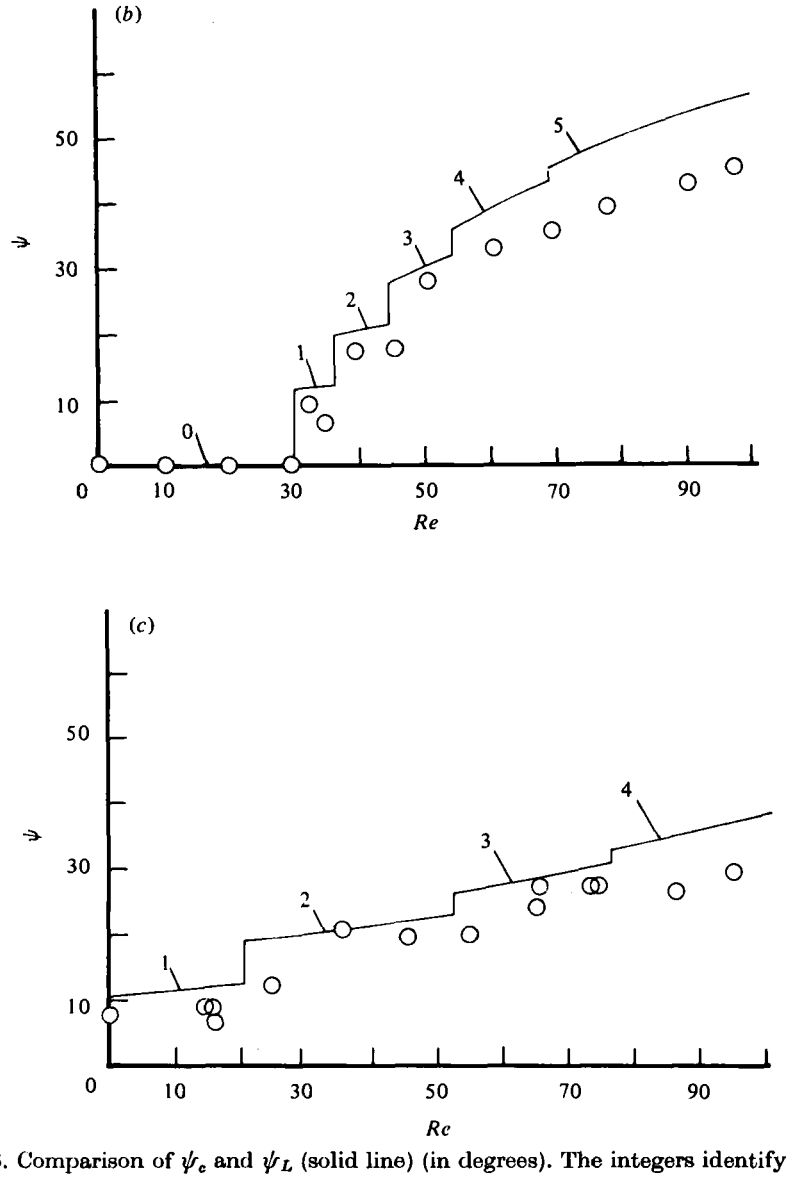

FIGURE 6. Comparison of ψ_c and ψ_L (solid line) (in degrees). The integers identify values of the azimuthal wavenumber; (*a*) $\mu = 0$; (*b*) $\mu = 0{\cdot}2$; (*c*) $\mu = -0{\cdot}5$.

for Ta_L. These results are tabulated in table 3. For $\mu = 0$, agreement between Ta_c and Ta_L extends to approximately $Re = 40$. Above this value, Ta_c is greater than Ta_L with the discrepancy increasing slightly with Re. Similar behaviour is noted for $\mu = 0{\cdot}2$ despite the large difference in the predictions for $\mu = 0$ and $0{\cdot}2$. In contrast, for $\mu = -0{\cdot}5$, Ta_c is consistently above Ta_L. Despite the markedly different behaviour of Ta_L with Re for the values of μ considered, the correct trends are indicated by Ta_c. In addition, there is a strong resemblance between the experimental results and 'scalloped' nature of the predicted curves. While there are no experimental results

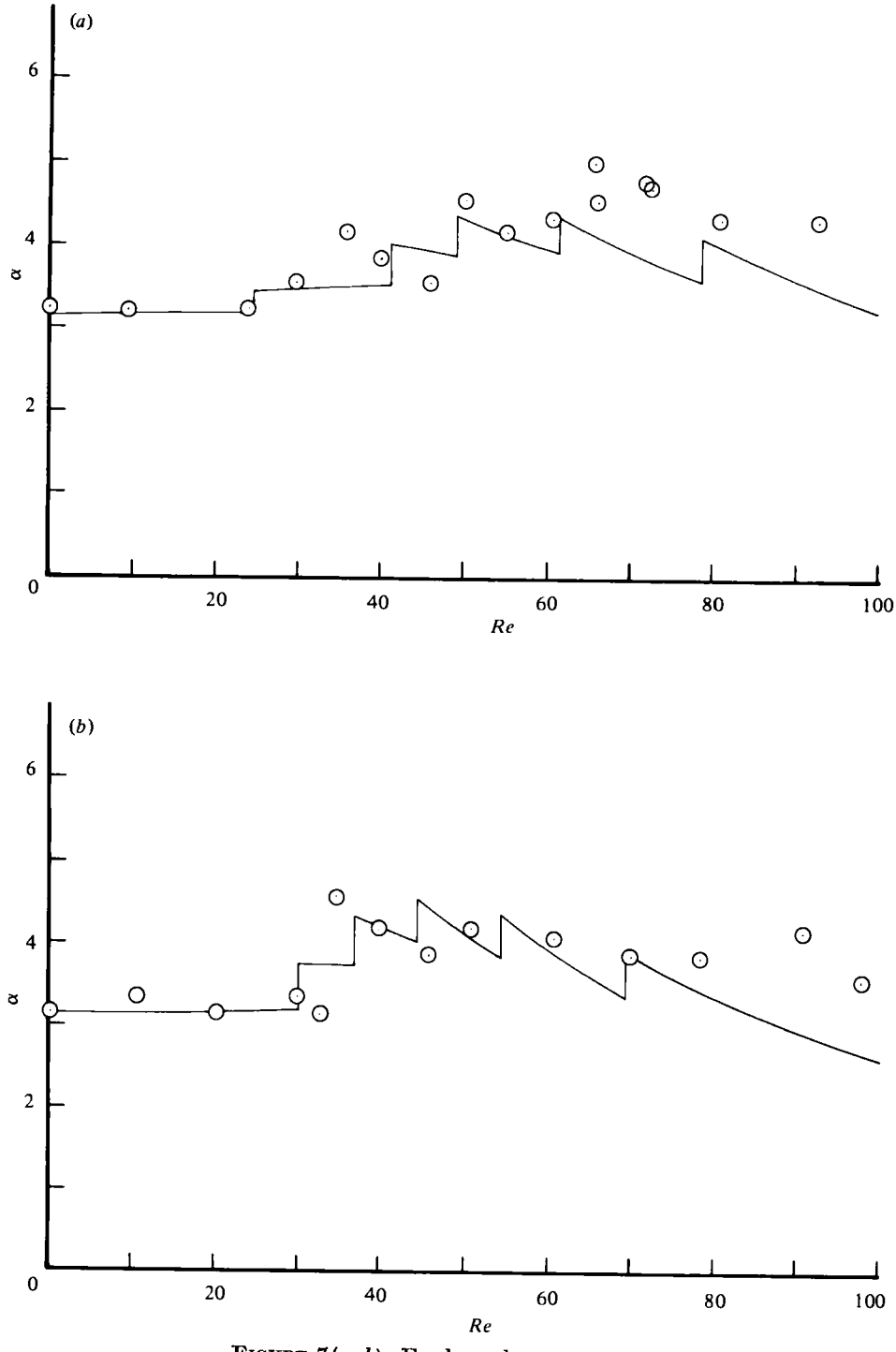

FIGURE 7(*a*, *b*). For legend see next page.

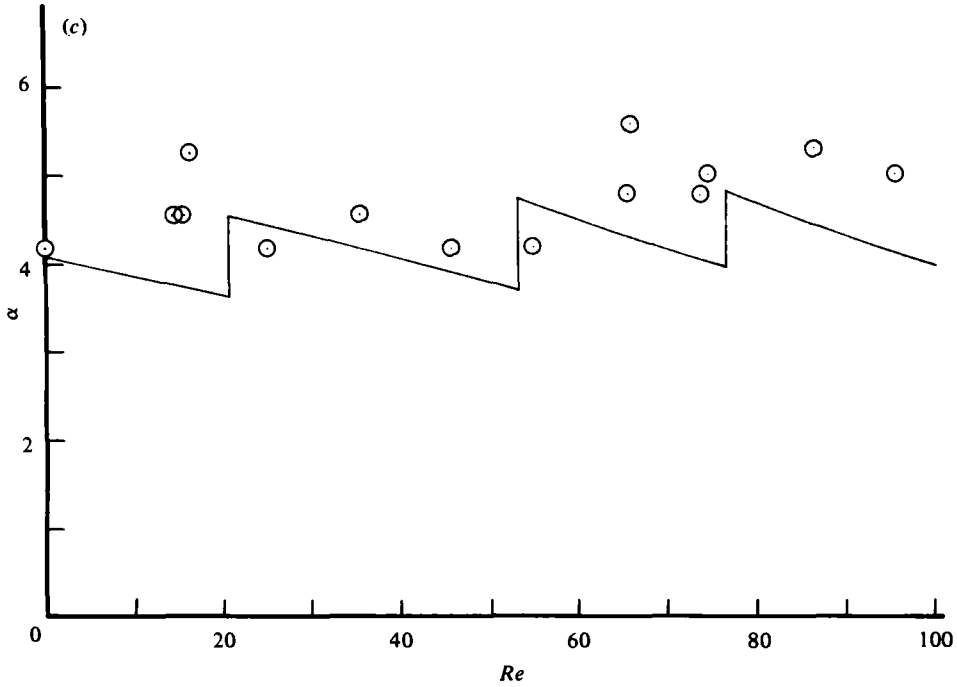

FIGURE 7. Comparison of α_c and α_L (solid line); (*a*) $\mu = 0$; (*b*) $\mu = 0{\cdot}2$; (*c*) $\mu = -0{\cdot}5$.

$\mu = 0$				$\mu = 0{\cdot}2$				$\mu = -0{\cdot}5$			
Re	ψ_c	α_c	n_c	Re	ψ_c	α_c	n_c	Re	ψ_c	α_c	n_c
0	0	3·24	0	0	0	3·14	0	0	7·5	4·19	0·70
9·4	0	3·24	0	10·0	0	3·35	0	14·1	9·0	4·57	0·92
23·7	0	3·24	0	19·9	0	3·14	0	15·2	9·0	4·57	0·92
29·4	9·0	3·59	0·72	29·6	0	3·35	0	16·0	6·5	5·29	0·77
35·7	7·6	4·19	0·71	32·3	9·0	3·14	0·63	24·9	12·0	4·19	1·13
39·6	8·0	3·87	0·69	34·2	6·2	4·57	0·63	35·3	20·5	4·56	2·18
45·5	11·3	3·59	0·91	39·3	17·2	4·19	1·65	45·6	19·4	4·19	1·88
49·7	16·6	4·57	1·73	45·4	17·8	3·87	1·58	54·9	19·9	4·19	1·93
54·9	19·0	4·19	1·84	50·4	28·0	4·19	2·84	65·3	24·0	4·79	2·71
60·3	24·6	4·37	2·55	60·4	33·0	4·19	3·46	65·7	27·0	5·59	3·62
65·3	23·0	5·03	2·72	69·7	35·2	3·87	3·47	73·6	27·2	4·79	3·13
65·9	26·0	4·57	2·83	78·1	39·0	3·87	3·99	74·7	27·3	5·03	3·30
71·5	29·0	4·79	3·38	90·4	42·8	4·19	4·94	86·3	26·4	5·29	3·34
71·8	30·0	4·79	3·52	97·7	45·0	3·59	4·57	95·3	29·5	5·03	3·62
80·3	31·3	4·37	3·38								
92·1	37·3	4·37	4·24								

TABLE 4. Experimental results for ψ_c (degrees), α_c, and n_c as a function of μ and Re.

available for a direct comparison, the present results for $\mu = 0$ seem consistent with similar results reported for $\eta = 0{\cdot}96$ (Snyder 1965) and $\eta = 0{\cdot}77$ (Mavec 1973).

Since there is an increasing difference between Ta_c and Ta_L as Re increases, the wave-form experiments were performed only for $Re \leqslant 100$. The experimentally determined ψ_c are shown in figure 6. These figures also display a predicted angle ψ_L which is calculated by means of (16). The occurrence of a change in the critical wave form from a toroidal to a spiral structure is clearly shown for $\mu = 0$ and $0{\cdot}2$. A different behaviour is observed for $\mu = -0{\cdot}5$ with a spiral structure present for all Re. These observations are in agreement with the predictions. Although the experimental results are consistently lower, trends are verified in all cases. Figure 7 displays the experimentally determined α_c and the corresponding α_L. Overall trends are again verified although the experimental data generally lies above the predictions. Both ψ_c and α_c show considerable local excursions from the predictions and discrete changes corresponding to changes in n_L are not discernible. The experimental results for ψ_c and α_c are tabulated together with the calculated n_c in table 4.

6. Discussion and conclusions

A reasonable extrapolation from the available results is that, for a wide gap, spiral Poiseuille flow would first exhibit instability above the linear stability limit for the range of Re considered. The predictions from linear stability theory and results of flow visualization experiments can be expected to agree if, in addition, instability leads to an equilibrium amplitude which can be observed *slightly* above the linear stability limit. While an equilibrium amplitude was always observed in the present work, its appearance was, in some cases, delayed until Ta was increased above Ta_L by a significant amount. This increase depends on Re and μ and exhibits a systematic behaviour. Since what is observed in experiments is finite behaviour, only a nonlinear theory can be expected to completely explain these observations. Although an appropriate nonlinear analysis is not available, reasons for the limited agreement between theory and experiment can be suggested. These reasons are most plausible for $\mu = 0$ and $0{\cdot}2$; similar influences should also be present for $\mu = -0{\cdot}5$, but they are not as readily apparent. It is clear that the choice of positive azimuthal wavenumbers cannot explain the difference between Ta_c and Ta_L. If negative values for n were relevant, still lower values for Ta_L would result (see (12)), thereby *increasing* the difference.

The most attractive explanation for the difference between Ta_L and Ta_c *at high* Re is the existence of a vortex development length, beyond the hydrodynamic entrance length. The vortex development length is the length needed for a moving disturbance to reach an amplitude that is observable by the visualization method. Since the portion of the test section available for this purpose decreases as Re increases (see figure 4), disturbances may leave the test section before reaching the threshold amplitude. When this limiting condition is reached, Ta_c must be increased above the value that would be appropriate in a longer apparatus in order to have an observable disturbance within the test section. When this occurs, Ta_c can be expected to be greater than Ta_L. In order to verify this idea, the apparatus was artificially shortened by masking the lower half of the test section and performing the experiments for $\mu = 0$. These results are included in figure 5(a). A comparison of the results for the

complete and 'shortened' apparatus clearly show the expected increase in Ta_c as the length of the apparatus is reduced.

Another factor which influences the determination of Ta_c can be attributed to the apparatus design and the slopes of the Ta_L *vs.* Re curves. The apparatus was designed to impose a constant pressure drop across the test section. Thus, once a vortex structure appears, the axial flow rate must decrease. For a negative slope ($dTa_L/dRe < 0$) this decrease moves the flow state toward a stable region and tends to delay the development of an observable disturbance amplitude. This implies that the flow visualization procedure is hindered for negative slopes. Unfortunately, the relative importance of this effect cannot be established since its results cannot be separated from those associated with the vortex development length. However, it is interesting to note the degree of correlation in figures 5(*a*) and 5(*b*) between disagreement and the existence of negative slopes.

The most significant feature of the comparison between the observed and predicted wave forms is the local excursions in the experimental data from overall trends. A possible explanation for this behaviour is suggested by experimental results due to Snyder (1969) who showed that, for unstable circular Couette flow, the observed wave form is uniquely determined by the initial conditions slightly below Ta_L. In the present work, the initial conditions for the determination of ψ_c and α_c were established at a state below Ta_c. In view of the behaviour of Ta_c and Ta_L, in some cases, this initial state was, in fact, *above* Ta_L. This situation may have affected the observed wave form. It is difficult to draw a definite conclusion because of the likely existence of additional complications due to the spiral form of the secondary flow. This thought is supported by the agreement shown in figures 7(*a*) and 7(*b*) for $n = 0$.

For a limited range of Re, the applicability of linear stability theory in determining the conditions for the onset of a non-axisymmetric secondary flow has been demonstrated for spiral Poiseuille flow in a wide-gap geometry. Detailed comparisons of the corresponding wavenumbers have been somewhat less successful, but general trends are in agreement. The existence of the vortex development length implies that the linear theory has an even greater range of applicability than demonstrated here. However the experimental determination of this range is hampered by serious difficulties in fabricating a sufficiently long test section for a wide-gap geometry. If the apparatus length does have an influence on the vortex development process, it can be concluded that a nonlinear analysis is necessary to determine the conditions under which a vortex structure will be observed.

It is a sincere pleasure to acknowledge the substantial contributions of Mr Frank Hombaker in the construction of the experimental apparatus. Professor R. C. DiPrima kindly provided a pre-publication copy of his paper. This work was supported in part (D.F.J.) by a grant from the University Grants Committee of Arizona State University.

REFERENCES

Chandrasekhar, S. 1960 *Proc. Nat. Acad. Sci.* **46**, 141–143.

Chandrasekhar, S. 1962 *Proc. Roy. Soc.* A **265**, 188–197.

Chung, K. C. & Astill, K. N. 1977 *J. Fluid Mech.* **81**, 641–655.

Coles, D. 1965 *J. Fluid Mech.* **21**, 385–425.

DATTA, S. L. 1965 *J. Fluid Mech.* **21**, 635–640.

DAVEY, A. 1962 *J. Fluid Mech.* **14**, 336–368.

DIPRIMA, R. C. 1960 *J. Fluid Mech.* **9**, 621–631.

DIPRIMA, R. C. & PRIDOR, A. 1979 *Proc. Roy. Soc.* A **366**, 555–573.

ELLIOTT, L. 1973 *Phys. Fluids* **16**, 577–580.

GRAVAS, N. & MARTIN, B. W. 1978 *J. Fluid Mech.* **86**, 385–394.

HASOON, M. A. & MARTIN, B. W. 1977 *Proc. Roy. Soc.* A **352**, 351–380.

HUGHES, T. H. & REID, W. H. 1968 *Phil. Trans. Roy. Soc.* A **263**, 57–91.

JOSEPH, D. D. & MUNSON, B. R. 1970 *J. Fluid Mech.* **43**, 545–575.

JOSEPH, D. D. 1976 *Stability of Fluid Motions I.* Springer.

KRUEGER, E. R. & DIPRIMA, R. C. 1964 *J. Fluid Mech.* **19**, 528–538.

KRUEGER, E. R., GROSS, A. & DIPRIMA, R. C. 1966 *J. Fluid Mech.* **24**, 521–528.

KUESTER, J. L. & MIZE, J. H. 1973 *Optimization Techniques with FORTRAN.* McGraw-Hill.

LANCE, G. N. 1959 *J. Assoc. Comput. Mach.* **6**, 208–215.

LESSEN, M., SINGH, P. J. & PAILLET, F. 1974 *J. Fluid Mech.* **63**, 753–763.

MACKRODT, P.-A. 1976 *J. Fluid Mech.* **73**, 153–164.

MARTIN, B. W. & HASOON, M. A. 1976 *J. Mech. Engng Sci.* **18**, 221–228.

MARTIN, B. W. & PAYNE, A. 1972 *Proc. Roy. Soc.* A **328**, 123–141.

MASLOWE, S. A. 1974 *J. Fluid Mech.* **64**, 307–317.

MAVEC, J. A. 1973 Spiral and toroidal secondary motions in swirling flows through an annulus at low Reynolds number. M.S.E. thesis, Illinois Institute of Technology.

MOTT, J. E. & JOSEPH, D. D. 1968 *Phys. Fluids* **11**, 2065–2073.

MULLER, D. E. 1956 *Math. Comp.* **10**, 208–215.

NAGIB, H. M. 1972 On instabilities and secondary motions in swirling flows through annuli. Ph.D. thesis, Illinois Institute of Technology.

ROBERTS, P. H. 1965 *Proc. Roy. Soc.* A **283**, 550–555.

SCHWARZ, K. W., SPRINGETT, B. E. & DONNELLY, R. J. 1964 *J. Fluid Mech.* **20**, 281–289.

SNYDER, H. A. 1962 *Proc. Roy. Soc.* A **265**, 198–214.

SNYDER, H. A. 1965 *Ann. Phys.* **31**, 292–313.

SNYDER, H. A. 1969 *J. Fluid Mech.* **35**, 273–298.

SPARROW, E. M. & LIN, S. H. 1964 *Trans. A.S.M.E.* D, *J. Basic Engng*, **86**, 827–834.

SPARROW, E. M., MUNRO, W. D. & JONSSON, V. K. 1964 *J. Fluid Mech.* **20**, 35–46.

TAKEUCHI, D. I. 1979 A numerical and experimental investigation of the stability of spiral Poiseuille flow. Ph.D. thesis, Arizona State University.